Research Article
Fault Tolerant Control Algorithm of Hexarotor UAV

Songming Jiao, Haiyue Gao, Xiaokun Zheng [ID], and Dengpan Liu

Department of Automation, North China Electric Power University, Baoding 071003, China

Correspondence should be addressed to Xiaokun Zheng; 56704037@qq.com

As the best representative of the current cutting-edge technology, unmanned aerial vehicle (UAV) is widely used in various fields such as electric power inspection, agriculture, forestry and plant protection, fire rescue, and film and television shooting. With the rapid development of UAV, the safety work of UAV has become more important. In order to improve the safety of hexarotor UAV during flight, a fault-tolerant control scheme independent of basic control law and control distribution is designed in this paper. Firstly, the linear active disturbance rejection control (LADRC) was used as the basic control law for attitude control of hexarotor UAV. Secondly, in the case of actuator failure of hexarotor UAV, a fault observer was used to estimate fault information accurately. Then, on this basis, the control distribution matrix was adjusted to reduce the use of the faulty motor, and the purpose of fault-tolerant control was achieved. Finally, simulation experiments and actual flight experiments were carried out to verify the effectiveness of the proposed scheme. Experimental results show that the proposed scheme can improve the robustness of the control system and the flight safety of UAV.

1. Introduction

In recent years, with the continuous progress of science and technology, unmanned aerial vehicles (UAVs) have also made rapid development, especially in the field of multirotor UAV. Multirotor UAV is an aircraft equipped with airborne equipment such as data processing and transmission systems, sensors, automatic control systems, and communication systems. It can perform certain steady-state control and flight and has certain autonomous flight capabilities [1]. Multirotor aircrafts have been widely used in agriculture, forestry, plant protection, power inspection, logistics, and transportation, which have greatly facilitated people's production and life. Among them, the quadrotor UAV and the hexarotor UAV occupy a large proportion. However, due to the lack of redundancy of the rotor components of the quadrotor UAV, once the transmission failure occurs, the flight attitude changes abruptly, which will cause inestimable consequences in some application areas. As for the hexarotor UAV, due to the redundant actuators in the system, the optimized control algorithm can enable the hexarotor UAV to have good fault tolerance, greater load capacity, and higher stability, so as to complete more complex tasks.

Therefore, it is of great significance to study the fault-tolerant control of the hexarotor UAV.

The hexarotor UAV has the characteristics of high nonlinearity, strong coupling, and difficulty in modeling. To study the fault-tolerant control of the hexarotor UAV, it is necessary to choose a basic control law with certain robustness. Chen et al. [2] proposed a UAV control system based on the integral sliding mode, and the control system has certain immunity. Ma [3] designed a UAV control system based on the active disturbance rejection controller and realized the attitude control of the UAV through the active disturbance rejection control (ADRC). As the ADRC controller does not rely on the precise mathematical model of the controlled object and is easy to implement, the control system is robust.

Next, equally important is the fault-tolerant control. Cao et al. [4] took the missile as the research object and designed a fault-tolerant control of the actuator based on compensation. Wang and Ni [5] proposed a fault diagnosis method of the actuator based on an adaptive observer, which provided relatively accurate fault information for fault-tolerant control. Nguyen and Hong [6] proposed a conventional adaptive sliding mode control method for chattering and

system uncertainty to realize fault-tolerant control of UAV. In [7], a hardware circuit is designed to estimate the actuator fault for the hexarotor UAV. Finally, the control distribution matrix is calculated for different types of actuator fault, and the fault-tolerant control is realized.

Based on the above analysis, this paper takes the "X" hexarotor UAV as the research object and proposes a fault-tolerant control scheme for the hexarotor UAV based on control distribution.

The rest of this work is structured as follows: In Section 2, some related works on hexarotor UAV fault-tolerant control strategies are presented. In order to carry out simulation experiments, we have established mathematical models of the hexarotor UAV under normal conditions and fault conditions. Then, Section 3 provides some technical details about the UAV used to deploy our proposal, highlighting the basic control law based on linear active disturbance control (LADRC) and fault-tolerant control law based on control distribution. The main results are then presented in Section 4, which are the results of simulation experiments and actual flight experiments. Finally, Section 5 concludes this work and refers to future works.

2. UAV Modeling

2.1. UAV Modeling Normal Condition. The kinematics and dynamics models of the "X" hexarotor UAV were established under normal conditions. The simplified structure of "X" hexarotor UAV is shown in Figure 1. Since the flight environment and movement mode of the hexarotor UAV are relatively complex, the following assumptions are made to simplify the modeling work for the convenience of analysis [8]:

(1) Assume that the mass of the hexarotor UAV is uniform, and the structure center of the hexarotor UAV is its centroid

(2) It is assumed that the hexarotor UAV is a rigid body, that is, its basic structure and propeller will not deform during flight

(3) It is assumed that the effects of the rotation and revolution of the Earth are not considered

(4) Hexarotor UAVs fly at low speeds, so the effect of air resistance is ignored

(5) Ignoring the gyro effect of the hexarotor

2.1.1. Dynamic Model. First of all, the coordinate system, pitch angle, roll angle, and yaw angle are defined. As shown in Figure 1(b), the x-axis of the body coordinate system points to the forward direction of the aircraft through the center of gravity of the body, the y-axis points to the left wing of the body through the center of gravity of the body, and the z-axis passes through the center of gravity of the aircraft, perpendicular to the x-axis and y-axis, pointing to the top of the aircraft.

The geodetic coordinate system is parallel to the geodetic horizontal plane pointing to the north, the y-axis is parallel to the geodetic horizontal plane pointing to the west, and the z-axis is perpendicular to the geodetic horizontal plane pointing upward.

Pitch (θ): the angle between the x-axis of the body coordinate system and the geodetic horizontal plane is positively downward.

Roll (φ): the angle between the z-axis of the body coordinate system and the geodetic vertical plane passing through the x-axis of the body coordinate system. When the plane flies to the right, the roll angle is positive.

Yaw (ψ): the angle between the x-axis of the body coordinate system between the projection on the geodetic horizontal plane and the x-axis in the geodetic coordinate system. The yaw angle is positive when the nose turns left.

The hexarotor UAV has 4 control channels, a roll angle control channel, a pitch angle control channel, a yaw angle control channel, and an altitude channel. The deflection of the three attitude angles of the UAV is caused by the combined external torque, as reported in [9].

The lift generated by each rotor is proportional to the square of its angular velocity:

$$F_i = b\Omega_i^2, \tag{1}$$

where b is the lift coefficient and Ω_i is the angular velocity of six motors.

The structure of the hexarotor UAV used in this paper is shown in Figure 1(a). The included angle between the rotors is 60°. Therefore, its roll, pitch, and yaw torques can be obtained separately.

Roll torque can be expressed as

$$U_R = \frac{1}{2} bl\left(\Omega_1^2 + \Omega_5^2 + \Omega_6^2 - \Omega_2^2 - \Omega_3^2 - \Omega_4^2\right), \tag{2}$$

where l is the distance between the center of rotors on the diagonal.

In equation (2), $\cos 60°$ is equal to $1/2$, representing the torque component of motors 1, 2, 4, and 5 on the x-axis in the frame of the body.

Pitch torque can be expressed as

$$U_P = \frac{\sqrt{3}}{2} bl\left(\Omega_4^2 + \Omega_5^2 - \Omega_1^2 - \Omega_2^2\right). \tag{3}$$

In equation (3), $\sin 60°$ is equal to $\sqrt{3}/2$, representing the torque component of motors 1, 2, 4, and 5 on the y-axis in the frame of the body.

Yaw torque can be expressed as

$$U_Y = d\left(\Omega_1^2 - \Omega_2^2 + \Omega_3^2 - \Omega_4^2 + \Omega_5^2 - \Omega_6^2\right), \tag{4}$$

where d is the reverse torque coefficient.

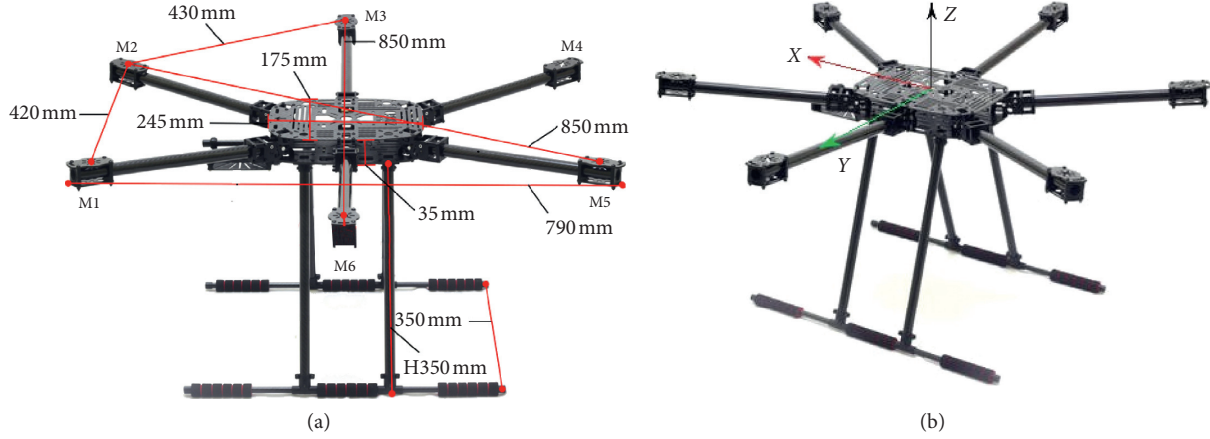From what has been discussed above, roll, pitch, and yaw torques can be expressed as

FIGURE 1: Information of the "X" hexarotor UAV: (a) simplified structure of the "X" hexarotor UAV and (b) coordinate system of the "X" hexarotor UAV.

$$\begin{bmatrix} U_R \\ U_P \\ U_Y \end{bmatrix} = \begin{bmatrix} \dfrac{1}{2}bl\left(\Omega_1^2 + \Omega_5^2 + \Omega_6^2 - \Omega_2^2 - \Omega_3^2 - \Omega_4^2\right) \\ \dfrac{\sqrt{3}}{2}bl\left(\Omega_4^2 + \Omega_5^2 - \Omega_1^2 - \Omega_2^2\right) \\ d\left(\Omega_1^2 - \Omega_2^2 + \Omega_3^2 - \Omega_4^2 + \Omega_5^2 - \Omega_6^2\right) \end{bmatrix}. \tag{5}$$

Equation (5) is the external closing torque of the hexarotor UAV. In equation (5), $U_R, U_P,$ and U_Y are roll torque, pitch torque and yaw torque, respectively.

From equation (5), we can get the following formula:

$$V = \begin{bmatrix} U_R \\ U_P \\ U_Y \end{bmatrix} = \begin{bmatrix} \dfrac{bl}{2} & -\dfrac{bl}{2} & -bl & -\dfrac{bl}{2} & \dfrac{bl}{2} & bl \\ -\dfrac{\sqrt{3}\,bl}{2} & -\dfrac{\sqrt{3}\,bl}{2} & 0 & \dfrac{\sqrt{3}\,bl}{2} & \dfrac{\sqrt{3}\,bl}{2} & 0 \\ d & -d & d & -d & d & -d \end{bmatrix} \begin{bmatrix} \Omega_1^2 \\ \Omega_2^2 \\ \Omega_3^2 \\ \Omega_4^2 \\ \Omega_5^2 \\ \Omega_6^2 \end{bmatrix}. \tag{6}$$

The torque balance experienced by the hexarotor UAV can be expressed as Newton–Euler's formula as follows:

$$I\dot{\omega} = -\omega \times I\omega + V. \tag{7}$$

According to equations (5) and (7), it can be obtained that

$$\begin{cases} \dot{p} = \dfrac{U_R + (I_y - I_z)qr}{I_x}, \\[2ex] \dot{q} = \dfrac{U_P + (I_z - I_x)pr}{I_x}, \\[2ex] \dot{r} = \dfrac{U_R + (I_x - I_y)pq}{I_x}, \end{cases} \tag{8}$$

where I is the torque of inertia of the hexarotor UAV about the triaxial axis of its carrier coordinate system, ω is the triaxial angular velocity of the hexarotor UAV about the carrier coordinate system, and V is the controlled quantity of three channels of roll, pitch, and yaw the amount.

Because the hexarotor UAV generally only performs small-angle motion, the Euler angle generated by the moment during flight is small, so the Euler angular velocity of the fuselage is approximately equal to the angular velocity of the fuselage coordinate system [10], that is,

$$\begin{bmatrix} \dot{\varphi} & \dot{\theta} & \dot{\psi} \end{bmatrix}^T \approx \begin{bmatrix} p & q & r \end{bmatrix}^T. \tag{9}$$

In summary, the dynamic model of a hexarotor UAV can be expressed as

$$\begin{cases} \ddot{\varphi} = \dfrac{U_R + (I_y - I_z)\dot{\theta}\dot{\psi}}{I_x}, \\[2ex] \ddot{\theta} = \dfrac{U_P + (I_y - I_z)\dot{\varphi}\dot{\psi}}{I_x}, \\[2ex] \ddot{\psi} = \dfrac{U_Y + (I_y - I_z)\dot{\theta}\dot{\varphi}}{I_x}. \end{cases} \tag{10}$$

2.1.2. Kinematic Model. The main forces of the hexarotor UAV include the gravity of the aircraft itself and the lift generated by the rotation of each propeller. The combined direction of the six lifts is perpendicular to the surface of the propeller disc and opposite to gravity.

Therefore, the total lift of the hexarotor UAV is

$$\begin{aligned} U_T = F &= F_1 + F_2 + F_3 + F_4 + F_5 + F_6 \\ &= b\left(\Omega_1^2 + \Omega_2^2 + \Omega_3^2 + \Omega_4^2 + \Omega_5^2 + \Omega_6^2\right). \end{aligned} \tag{11}$$

From Newton's second law of motion, $F = ma$, the kinematic model of the hexarotor UAV can be obtained as

$$\ddot{P} = \frac{R_b^e F + F_g}{m}. \tag{12}$$

$P = \begin{bmatrix} x & y & z \end{bmatrix}^T$ is the position vector of the UAV in the geodetic coordinate system, $\ddot{P}$ is the position acceleration vector of the UAV in the geodetic coordinate system, F_g is the triaxial gravity component of the hexarotor UAV in the geodetic coordinate system, and R_b^e is attitude conversion

matrix from the geodetic coordinate system to the body coordinate system.

There are three main kinds of attitude calculation algorithms that are widely used nowadays: the quaternion method, Euler angles, and rotation matrix method [11, 12]. The quaternion method is most widely used in the field of engineering. Its calculation is relatively small, and this method is also used in the UAV attitude calculation.

$$R_b^e = \begin{bmatrix} \cos\psi\cos\theta & \sin\psi\cos\theta & -\sin\theta \\ \cos\psi\sin\theta\sin\varphi - \sin\psi\cos\varphi & \sin\psi\sin\theta\sin\varphi + \cos\psi\cos\varphi & \cos\theta\sin\varphi \\ \cos\psi\sin\theta\cos\varphi + \sin\psi\sin\varphi & \sin\psi\sin\theta\cos\varphi - \cos\psi\sin\varphi & \cos\theta\cos\varphi \end{bmatrix}. \tag{13}$$

$F = \begin{bmatrix} 0 & 0 & U_T \end{bmatrix}^T$ is the total lift force of all rotors of the hexarotor UAV.

In summary, the kinematic model of a hexarotor UAV can be expressed as

$$\begin{bmatrix} \ddot{x} \\ \ddot{y} \\ \ddot{z} \end{bmatrix} = \begin{bmatrix} \dfrac{(\cos\psi\sin\theta\cos\varphi + \sin\psi\sin\varphi)U_T}{m} \\[2mm] \dfrac{(\sin\varphi\sin\theta\cos\varphi + \cos\psi\sin\varphi)U_T}{m} \\[2mm] \dfrac{(\cos\theta\cos\varphi)U_T - mg}{m} \end{bmatrix}. \tag{14}$$

The mathematical model of a hexarotor UAV under normal conditions can be summarized by equations (10) and (14):

$$\begin{cases} \ddot{x} = \dfrac{(\cos\psi\sin\theta\cos\varphi + \sin\psi\sin\varphi)U_T}{m}, \\[3mm] \ddot{y} = \dfrac{(\sin\varphi\sin\theta\cos\varphi + \cos\psi\sin\varphi)U_T}{m}, \\[3mm] \ddot{z} = \dfrac{(\cos\theta\cos\varphi)U_T - mg}{m}, \\[3mm] \ddot{\varphi} = \dfrac{U_R + (I_y - I_z)\ddot{\theta}\ddot{\psi}}{I_x}, \\[3mm] \ddot{\theta} = \dfrac{U_P + (I_y - I_z)\ddot{\varphi}\ddot{\psi}}{I_x}, \\[3mm] \ddot{\psi} = \dfrac{U_Y + (I_y - I_z)\ddot{\theta}\ddot{\varphi}}{I_x}. \end{cases} \tag{15}$$

2.2. UAV Modeling under Fault Condition. The main fault types of the UAV are rotor fault, motor fault, sensor fault, control signal loss, and so on. Among them, rotor fault and

motor fault are collectively referred to as actuator fault. Actuator fault is common and most important for UAV flight safety, so this paper mainly discusses the actuator fault of the hexarotor UAV.

When the hexarotor UAV is flying normally, the force efficiency of the actuator is 100%. When the actuator fails, the force efficiency of the UAV actuator is k. When $k = 0$, the actuator of the hexarotor UAV fails completely, and the efficiency is 0. When $k = 1$, the hexarotor UAV is faultless and flying normally. When $0 < k < 1$, the actuator of the hexarotor UAV partly fails, and the output is insufficient.

Take the motor fault as an example. Suppose motor No. 1 is faulty. Ω_i is the speed output of motor No. 1 without fault, which is constant, and Ω_i^f is the speed output of motor No. 1 with fault. Then, the mathematical expression of the motor fault is

$$\Omega_i^f = k\Omega_i. \tag{16}$$

The lift and counter torque generated by the faulty motor at this time can be obtained as follows:

$$\begin{aligned} F_i^f &= b\left(\Omega_i^f\right)^2 = bk^2\Omega_i^2, \\ Q_i^f &= d\left(\Omega_i^f\right)^2 = dk^2\Omega_i^2, \end{aligned} \tag{17}$$

where F_i^f is the lift generated by the faulty motor at this time and Q_i^f is the counter torque generated at this time.

At this point, the torque balance equation is

$$I\dot{\omega}^f = -\omega^f \times I\omega^f + V^f, \tag{18}$$

where ω^f is the triaxial acceleration of the UAV under fault state and V^f is the input torque matrix of the UAV under the fault state.

When the actuator of the hexarotor UAV fails, it can be converted into the loss of control input of four channels including roll, pitch, yaw, and altitude [13]. Then, the mathematical model of the hexarotor UAV under the fault state is as follows:

$$\begin{cases} \ddot{x} = \dfrac{(\cos\psi\sin\theta\cos\varphi + \sin\psi\sin\varphi)U_T}{m}, \\[3mm] \ddot{y} = \dfrac{(\sin\varphi\sin\theta\cos\varphi + \cos\psi\sin\varphi)U_T}{m}, \\[3mm] \ddot{z} = \dfrac{(\cos\theta\cos\varphi)U_T - mg}{m} - f_Z, \\[3mm] \ddot{\varphi} = \dfrac{U_R + (I_y - I_z)\dot{\theta}\dot{\psi}}{I_x} - f_R, \\[3mm] \ddot{\theta} = \dfrac{U_P + (I_y - I_z)\dot{\varphi}\dot{\psi}}{I_x} - f_P, \\[3mm] \ddot{\psi} = \dfrac{U_Y + (I_y - I_z)\dot{\theta}\dot{\varphi}}{I_x} - f_Y, \end{cases} \tag{19}$$

where $f_Z, f_R, f_P,$ and f_Y are the control losses of the altitude, roll, pitch, and yaw channels.

3. Control Law Design

The control law design is mainly divided into two parts: basic control law design and fault-tolerant control law design. These two parts are designed independently, which greatly simplify the fault-tolerant control process of UAV.

3.1. Basic Control Law Design. The core of ensuring the stable flight of a hexarotor UAV under normal circumstances is to design a basic control law with certain robustness. As linear active disturbance control (LADRC) has the characteristics of not relying on the precise mathematical model of the controlled object and is easy to implement, this paper adopts the improved attitude control algorithm of LADRC to control the flight of UAV, so as to ensure the robustness of UAV in the flight process.

The LADRC controller is mainly divided into two parts: the transition process-tracking differentiator (TD) and a linear extended state observer (LESO).

Firstly, this paper introduces the transition process.

In LADRC, we use a second-order isovolumetric link instead of the tracking differentiator as the transition process. In PID control, when the input of the system is a step signal, the input "jumps." However, the output of the system is dynamic inertia and cannot jump, so a transition process is arranged to convert the input from a jump to a slow change. Therefore, the second-order isovolumetric link can fully meet the requirements of the transition process, effectively solving the contradiction between "fastness" and "overshooting" of the PID controller. The commonly used second-order link is shown in equation (20). In the equation, T can be 1/50~1/10 of the expected transition time.

$$G(s) = \frac{1}{T^2 s^2 + 2Ts + 1}. \tag{20}$$

Secondly, this paper introduces the LESO [14]. This is the core part of the LADRC, which can track the variables of the system in real time.

Generally, when ignoring the higher-order characteristics of a linear controlled object, its mathematical model is as follows:

$$\ddot{y} + a_1 \dot{y} + a_2 y = w + bu. \tag{21}$$

The above formula can be transformed into

$$\ddot{y} = -a_1 \dot{y} - a_2 y + w + (b - b_0) + b_0 u = f(y, \dot{y}, w), \tag{22}$$

where u is the input, y is the output, w is the external disturbance, a_1 and a_2 are the system parameters, and b is the control gain, $b \approx b_0$.

The state space equation of the system is established to realize the real-time tracking of variables in the model:

$$\begin{cases} \dot{x_1} = x_2, \\ \dot{x_2} = x_3 + b_0 u, \\ \dot{x_3} = h, \\ y = x_1, \end{cases} \tag{23}$$

where x_1, x_2 and x_3 are the state variables of the system, $h = f(y, \dot{y}, w)$.

The linear extended state observer can be established as follows:

$$\begin{cases} \dot{z_1} = z_2 - \beta_1 (z_1 - y), \\ \dot{z_2} = z_3 - \beta_2 (z_1 - y) + b_0 u, \\ \dot{z_3} = -\beta_3 (z_1 - y). \end{cases} \tag{24}$$

By selecting the appropriate observer gain, β_1, β_2, and β_3, the linearly expanded state observer can achieve real-time tracking of each variable in the system, thus ensuring the stability of attitude control.

3.2. Tolerant-Control Law Design. Based on Section 2.2, the mathematical model of the hexarotor UAV is summarized. Based on this, this paper designs a fault-tolerant control law to ensure the stable flight of the hexarotor UAV when the actuator fails.

The idea of controlling distribution is as follows:

Given the virtual control amount (torque), the actual input (motor speed) of each actuator is obtained through mapping to obtain the desired output. Figure 2 shows the basic structure of control distribution.

In Figure 2, R is the input of the entire control loop, which is the desired attitude we need; V is the virtual control amount, that is, roll, pitch, and yaw torque; and y is the output of the entire control loop.

According to Section 2.1, the control efficiency matrix A of the hexarotor UAV under normal conditions can be obtained, which is determined by the hardware mechanical structure of the hexarotor UAV, mainly by the wheelbase, lift
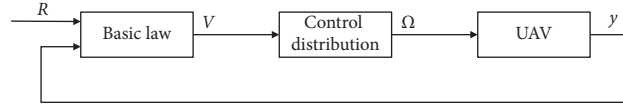
FIGURE 2: Block diagram of control distribution structure.

TABLE 1: Hexarotor UAV simulation structure parameter table.

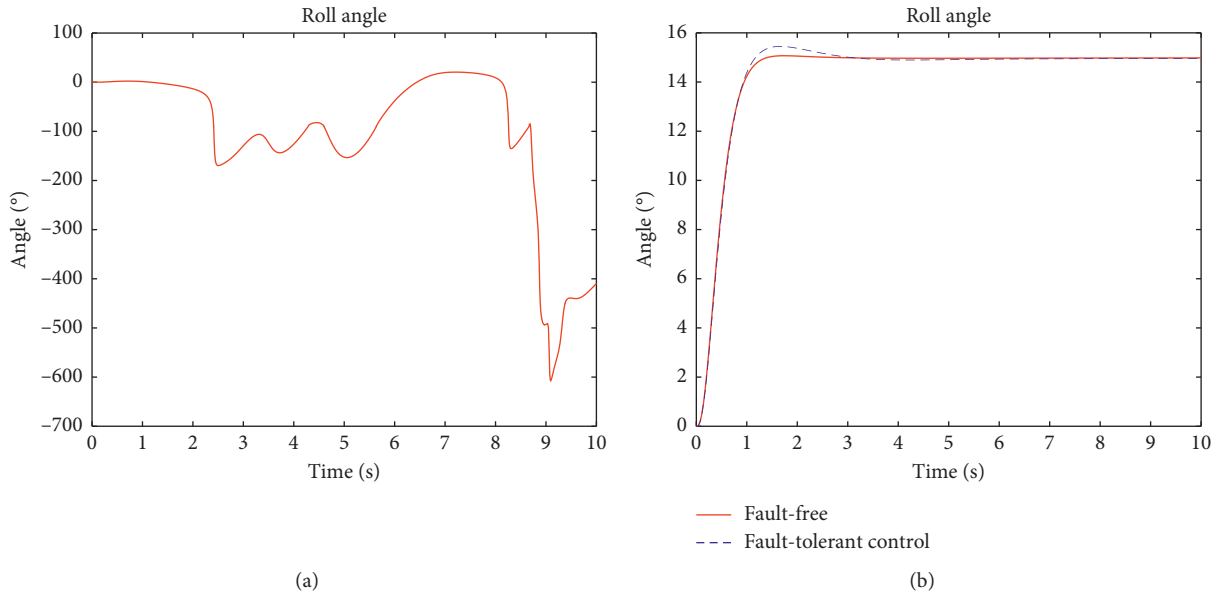| Parameter	Physical meaning	Value (kg·m^2)
I_x	Moment of inertia about x-axis	0.0135
I_y	Moment of inertia about y-axis	0.0135
I_z	Moment of inertia about z-axis	0.0268

(a)

(b)

— Fault-free
--- Fault-tolerant control

FIGURE 3: Comparison diagram of the roll angle before and after fault-tolerant control. (a) Non-fault-tolerant control. (b) Fault-tolerant control.

coefficient, antitorque coefficient, and the included angle between the axes, $V = A\Omega^2$.

According to equation (6),

$$A = \begin{bmatrix} \dfrac{bl}{2} & -\dfrac{bl}{2} & -bl & -\dfrac{bl}{2} & \dfrac{bl}{2} & bl \\[2mm] -\dfrac{\sqrt{3}\,bl}{2} & -\dfrac{\sqrt{3}\,bl}{2} & 0 & \dfrac{\sqrt{3}\,bl}{2} & \dfrac{\sqrt{3}\,bl}{2} & 0 \\[2mm] d & -d & d & -d & d & -d \end{bmatrix}. \quad (25)$$

For the quadrotor UAV, the control distribution matrix under normal circumstances can be obtained by simply inverting the control efficiency matrix. However, for a hexarotor UAV, the control efficiency matrix A is non-singular, and the control assignment matrix of the hexarotor UAV cannot be obtained directly by inversion. Therefore, we obtain the normal control distribution matrix N of the hexarotor UAV by finding the pseudo-inverse, $N \in R^{6\times3}$.

$$N = A^T \left(AA^T \right)^{-1} = \begin{bmatrix} \dfrac{1}{6bl} & -\dfrac{\sqrt{3}}{6bl} & \dfrac{1}{6d} \\[2mm] -\dfrac{1}{6bl} & -\dfrac{\sqrt{3}}{6bl} & -\dfrac{1}{6d} \\[2mm] -\dfrac{1}{3bl} & 0 & \dfrac{1}{6d} \\[2mm] -\dfrac{1}{6bl} & \dfrac{\sqrt{3}}{6bl} & -\dfrac{1}{6d} \\[2mm] \dfrac{1}{6bl} & \dfrac{\sqrt{3}}{6bl} & \dfrac{1}{6d} \\[2mm] \dfrac{1}{3bl} & 0 & -\dfrac{1}{6d} \end{bmatrix}. \quad (26)$$
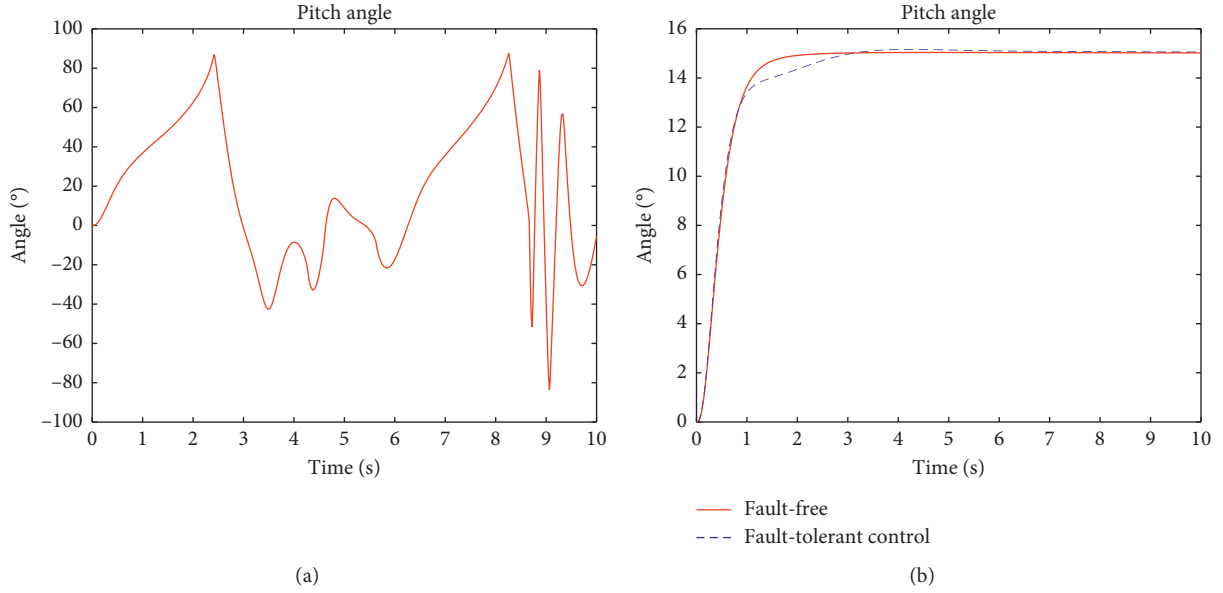
FIGURE 4: Comparison diagram of the pitch angle before and after fault-tolerant control. (a) Non-fault-tolerant control. (b) Fault-tolerant control.
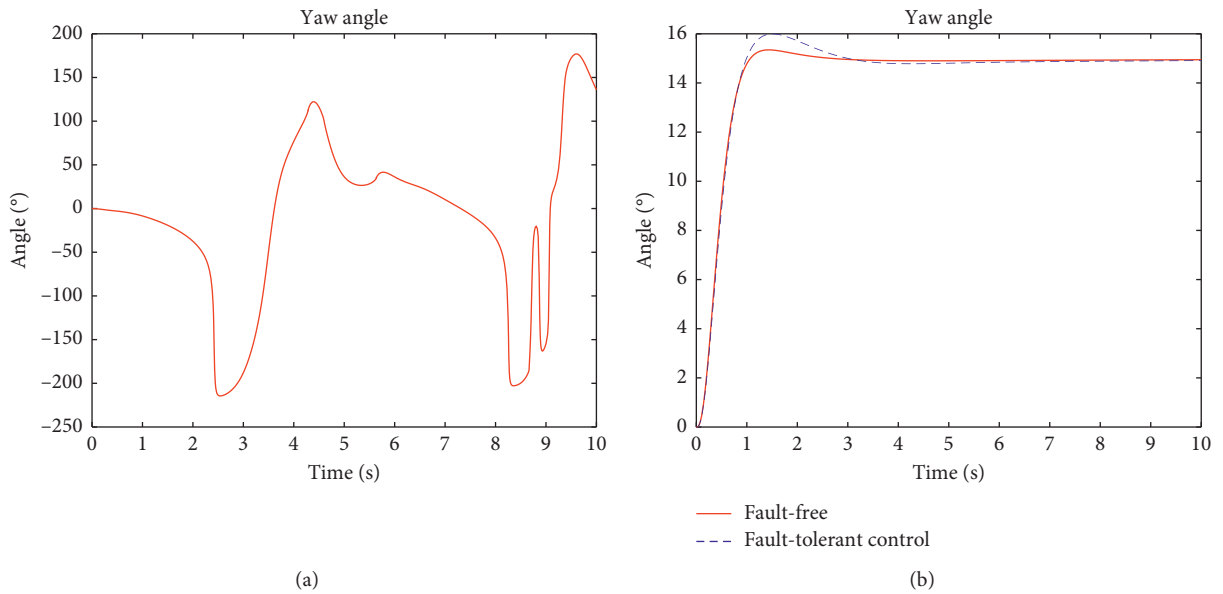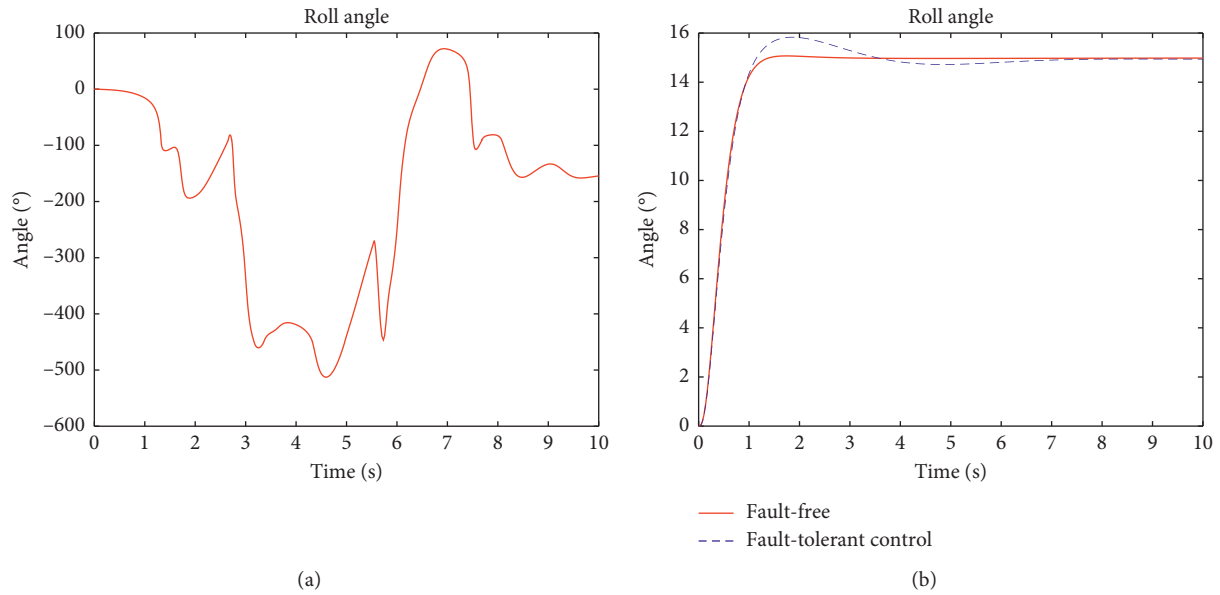

FIGURE 5: Comparison diagram of the yaw angle before and after fault-tolerant control. (a) Non-fault-tolerant control. (b) Fault-tolerant control.

Under normal fault-free conditions, the hexarotor UAV distributes the desired torque proportionally to the six motors through the control distribution matrix N. Upon the failure of the actuator, due to the insufficient output of the faulty motor, the torque required for flight cannot be achieved by using the normal pseudo-inverse control distribution method.

According to the obtained fault matrix, we need to use the pseudo-inverse weighting control algorithm to reduce the use of the fault motor and redistribute the remaining

motor to compensate the control quantity which is lost due to the insufficient output of a motor. At this time,

$$V_f = A\left(\Omega^f\right)^2 = AK\Omega^2, \tag{27}$$

where $K = \text{diag}\{k_1, k_2, \ldots, k_6\}$ is the fault matrix, $0 \leq k_i \leq 1$.

We set the weighted matrix as W. If the fault matrix K is known, the control distribution matrix can be adjusted as

$$N^f = WA^T\left(AWA^T\right)^{-1} = KA^T\left(AKA^T\right)^{-1}. \tag{28}$$

(a)   (b)

FIGURE 6: Comparison diagram of the roll angle before and after fault-tolerant control. (a) Non-fault-tolerant control. (b) Fault-tolerant control.

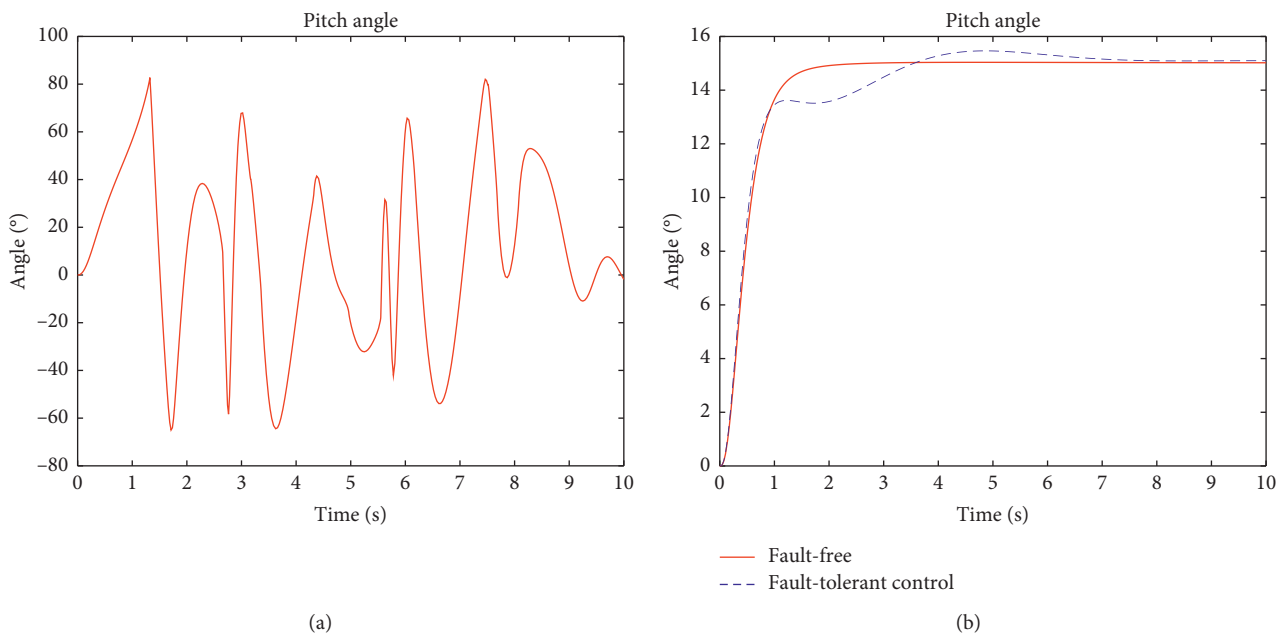(a)   (b)

FIGURE 7: Comparison diagram of the pitch angle before and after fault-tolerant control. (a) Non-fault-tolerant control. (b) Fault-tolerant control.

The above equation is the control distribution matrix adjusted according to the fault information.

4. Results and Discussion

4.1. Simulation Experiment Results. Based on the analysis and derivation in Section 3, a MATLAB simulation model for hexarotor UAV fault-tolerant control is established on the basis of the fault-free simulation model. The effectiveness of the fault-tolerant control scheme is verified by comparing the simulation control effects before and after the fault.

Due to the limitation of experimental conditions, the laboratory does not have some structural parameters. Therefore, the aerodynamic parameters such as the moment of inertia of the six-rotor drone involved in the simulation experiments in this paper mainly come from pertinent literature [15], lift coefficient, and antitorque coefficient given by the merchant. The main parameters are the mass of the
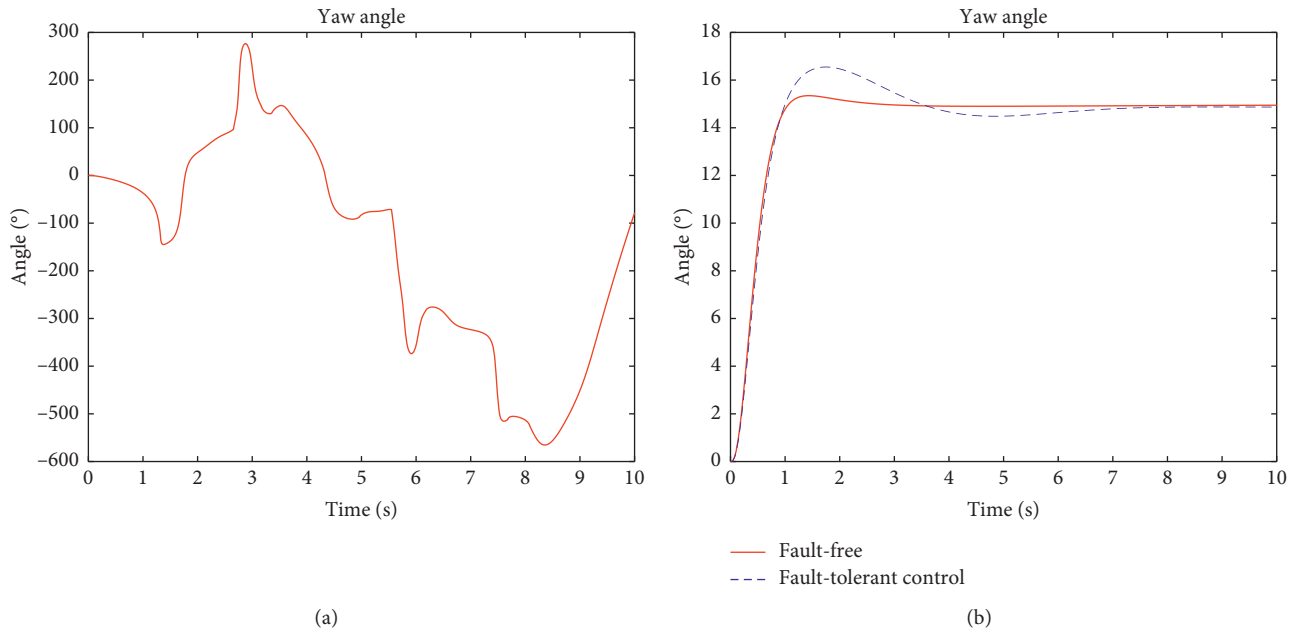
(a)

(b)

Figure 8: Comparison diagram of the yaw angle before and after fault-tolerant control. (a) Non-fault-tolerant control. (b) Fault-tolerant control.

Figure 9: Simple lift test device.
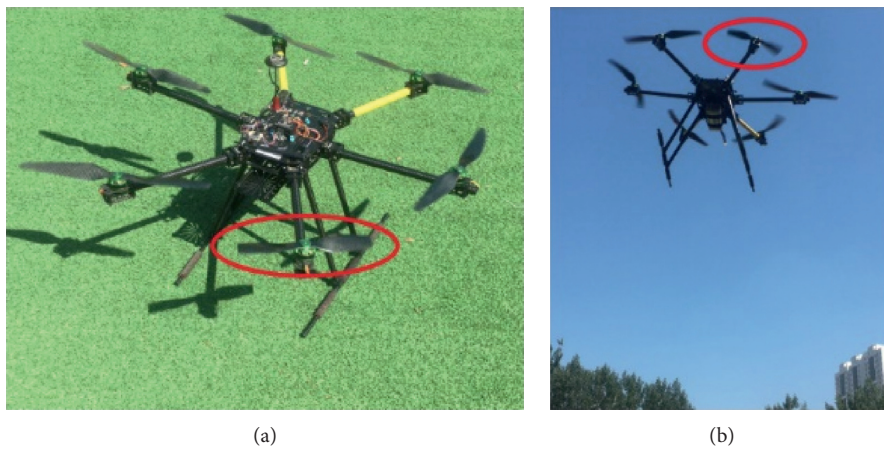

(a)

(b)

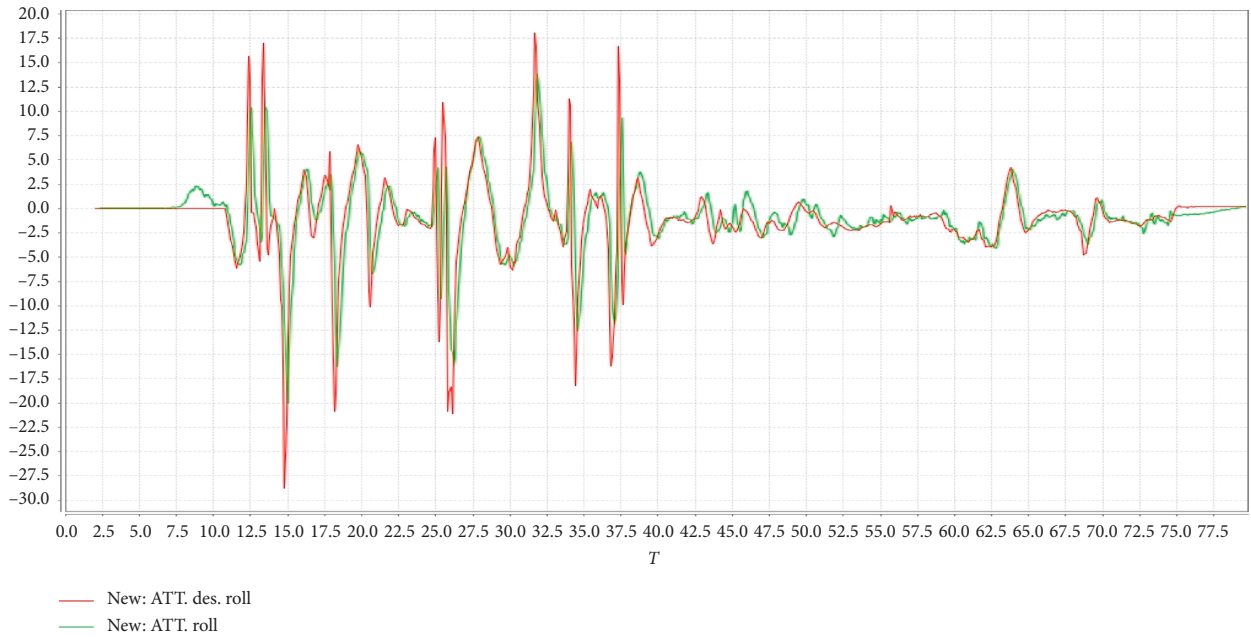Figure 10: Actual flight chart.
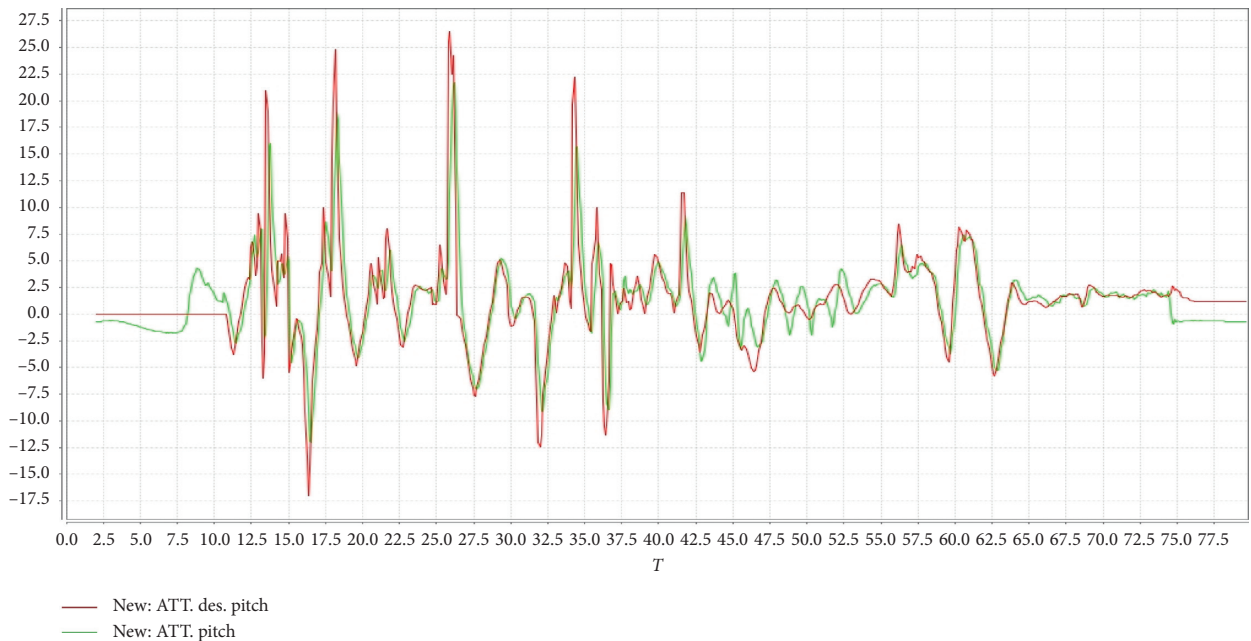
FIGURE 11: Actual flight roll angle graph.

FIGURE 12: Actual flight pitch angle graph.

hexarotor UAV, the distance between the center of the rotor and center of the mass, the lift coefficient, the antitorque coefficient, and the moment of inertia of the UAV when it moves around three axes. We set the mass of UAV as $m = 5\,\text{kg}$, the distance between the center of the rotor and the center of the mass as $l = 0.45\,\text{m}$, the gravitational acceleration as $g = 9.8\,\text{N/kg}$, the lift coefficient as $b = 0.0000542\,\text{N}\cdot\text{s}^2$, and the antitorque as

$D = 0.0000011\,\text{N}\cdot\text{ms}^2$. The moment of inertia of the hexarotor UAV built in this paper is shown in Table 1.

In this experiment, it is assumed that the initial values of roll angle, pitch angle, and yaw angle are $0°$, and the three expected attitude angles set are ($15°$, $15°$, and $15°$). If motor No. 1 fails and fails 50% and 70% of the time, the simulation test is conducted to verify whether the fault-tolerant control law can stabilize the expected value set by tracking.
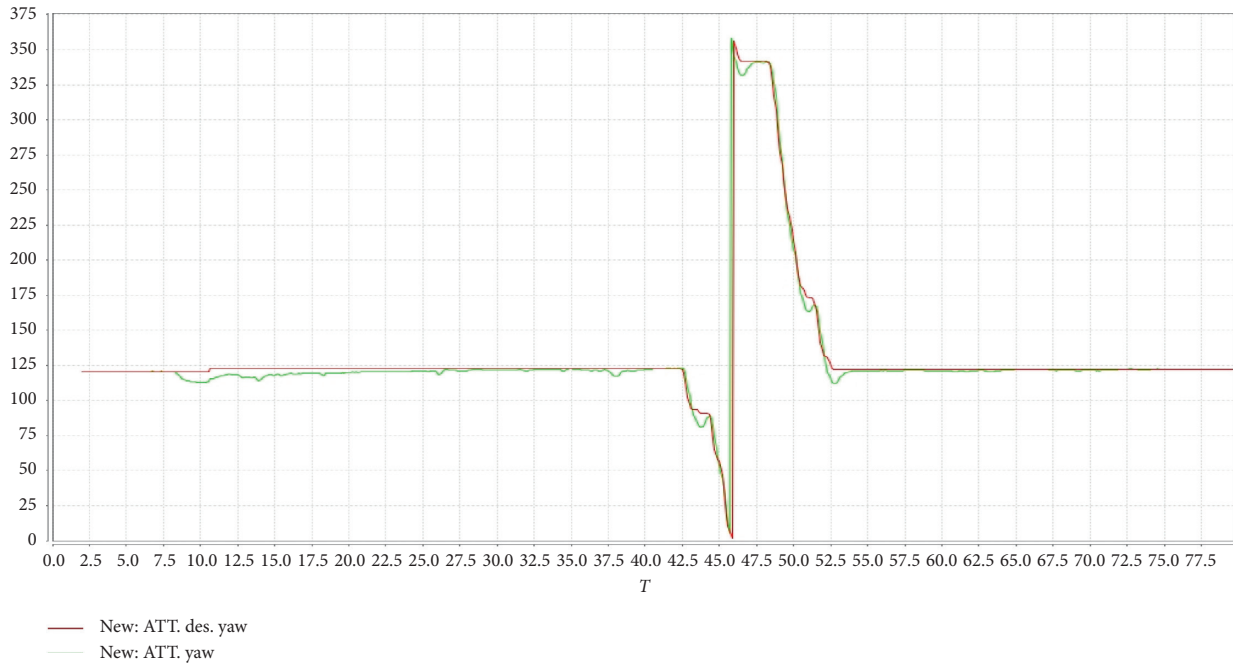
FIGURE 13: Actual flight yaw angle graph.

(a)

(b)

FIGURE 14: Actual flight chart.

The simulation results are shown in the following figures.

Figures 3–5 are the simulation curves when motor No. 1 fails 50%.

When the actuator failure of the hexarotor UAV occurs, the three attitude angle change curves are shown in Figures 3–5. As shown in Figures 3 to 5, (a) is the simulation curve without fault-tolerant control and (b) is the comparison curve of the simulation curve under no-fault condition and fault-tolerant control. It can be seen from the figures that when motor No. 1 of the hexarotor UAV fails 50%, that is, the power efficiency is 50%, and if there is no fault-tolerant control, the output result is too oscillating and cannot reach final stability. Under the fault-tolerant control scheme proposed in this paper, the hexarotor UAV can still track the expected value and reach the final stability.

Figures 6–8 are the simulation curves when motor No. 1 fails 70%.

When the actuator failure of the hexarotor UAV occurs, the three attitude angle change curves are shown in Figures 6–8. It can be seen from the figures that when motor No. 1 of the hexarotor UAV fails 70%, that is, the power efficiency is 30%, and if there is no fault-tolerant control, the output result is too oscillating and cannot reach final stability. Under the fault-tolerant control scheme proposed in this paper, the hexarotor UAV can still track the expected value and reach the final stability.

4.2. Actual Flight Experiment Results. Based on the simulation experiments, this chapter modified the APM source code according to the fault-tolerant control scheme designed above and burned it into a hexarotor drone to verify the effectiveness of the fault-tolerant control scheme.
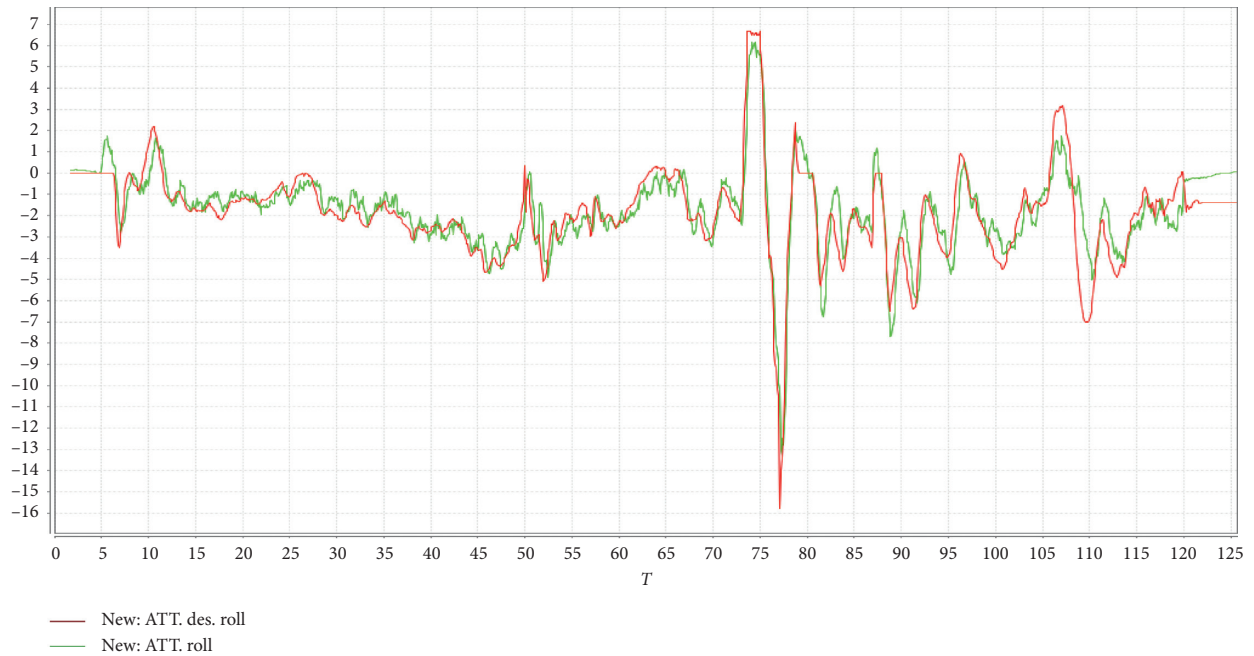
Figure 15: Actual flight roll angle graph.

Figure 16: Actual flight pitch angle graph.

Due to experimental conditions, this paper simulates motor failure by cutting off the rotor.

A simple hexarotor UAV propeller lift test is shown in Figure 9. The middle of the device consists of the remote control receiver, and one side consists of the propeller and the motor. By fixing the position of the throttle stick of the remote control and comparing the propeller lift without failure, the lift of the faulty propeller is obtained. After several experimental tests, the average value was obtained to obtain the power effect of the damaged propeller.

Figure 10 shows the flight experiment diagram when the propeller force effect is 50%. Instructions such as
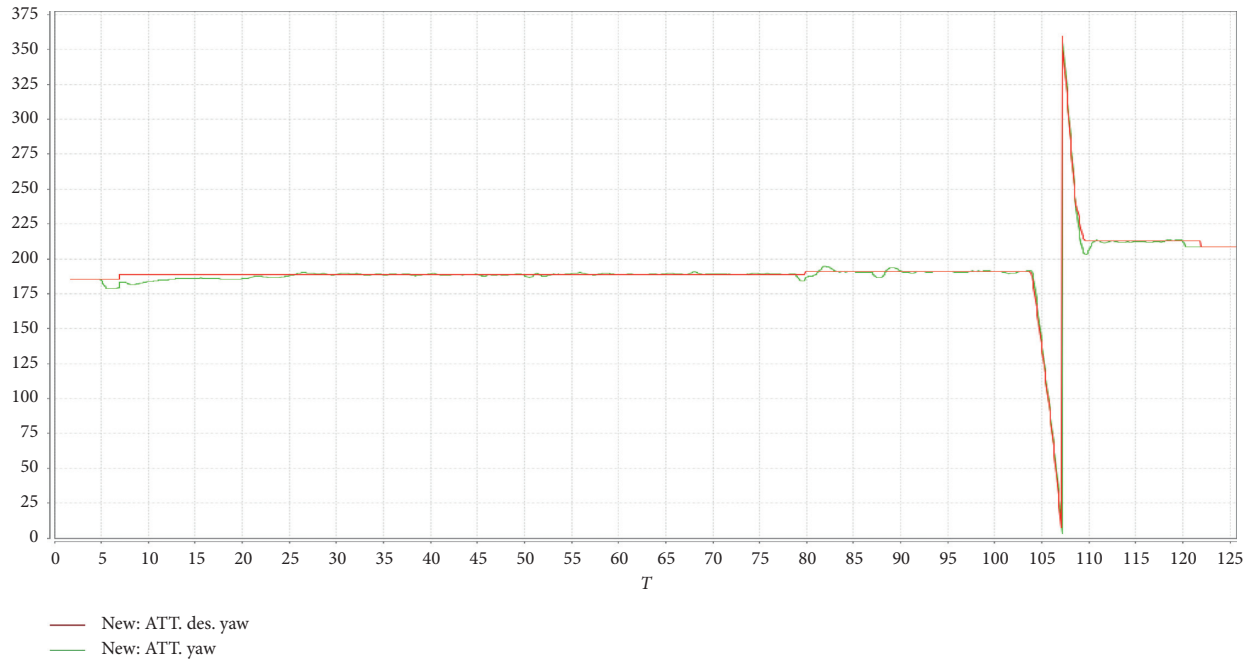
FIGURE 17: Actual flight yaw angle graph.

(a)　　　　　　　　　　　　　　　　　　　(b)

FIGURE 18: Actual flight chart.

take-off, hover, and attitude angle change are sent to the UAV through the remote control to observe the attitude change during the flight of the UAV, and then the flight data are analyzed through the MAVLINK flash log in the Mission Planner Earth station. In the Mission Planner ground station, the effect of the fault-tolerant control algorithm was verified mainly through the comparison between the expected attitude angle and the real-time attitude angle, as well as the oscillation degree of IMU and other sensors.

Figures 11–13 are the actual following curves of the three attitude angles when the propeller power efficiency is 50%. In these figures, the red curves represent the desired attitude angle, and the green curves represent the real-time attitude angle of the hexarotor UAV. It can be seen from the figures

that the hexarotor UAV can still track the changes of the 3 attitude angles well, and the vibration is small during flight.

Figure 14 shows the flight experiment diagram when the propeller force effect is 30%.

Figures 15–17 are the actual following curves of the three attitude angles when the propeller power efficiency is 30%. In these figures, the red curves represent the desired attitude angle, and the green curves represent the real-time attitude angle of the hexarotor UAV. It can be seen from the figures that the hexarotor UAV can also track the changes of the 3 attitude angles well, and the vibration is small during flight.

Finally, on the basis of the above experimental analysis, it is verified whether the fault-tolerant control scheme can still keep the six-rotor UAV stable after the complete removal of a propeller. Figure 18 shows the flight experiment.

FIGURE 19: Actual flight roll angle graph.

FIGURE 20: Actual flight pitch angle graph.

Figures 19–21 are the actual following curves of the three attitude angles when the propeller power efficiency is 0%. In these figures, the red curves represent the desired attitude angle, and the green curves represent the real-time attitude angle of the hexarotor UAV. It can be seen from the figures that the tracking effect of the UAV is not good during take-off and landing, and the actual attitude angle deviates from the expected attitude angle. However, in the process of flight, the UAV can better track the change of the attitude angle.
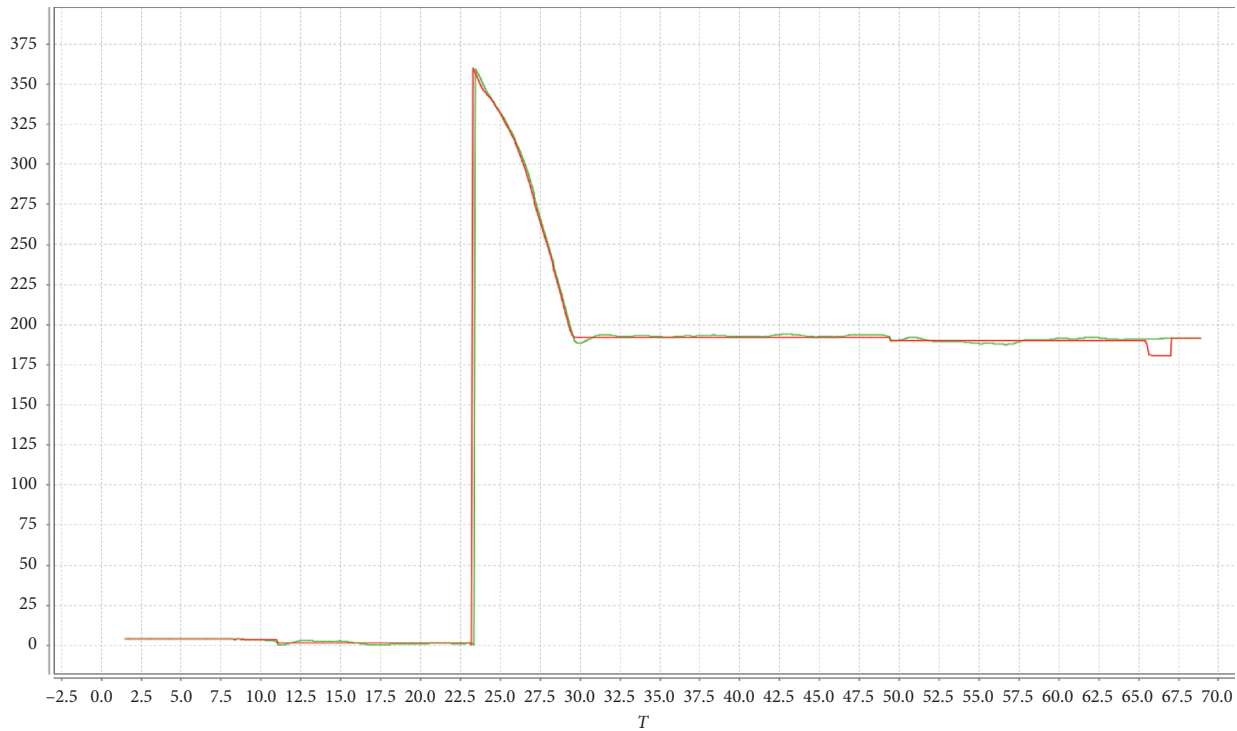
FIGURE 21: Actual flight yaw angle graph.

5. Conclusions

Compared with the quadrotor, the hexarotor unmanned aerial vehicle (UAV) has redundant actuators and a larger load capacity, so it has a stronger anti-interference ability, higher safety, and is able to adapt to more severe flight environment and complete more complex tasks. Therefore, this paper takes the hexarotor UAV as the experimental platform to carry out a series of research works.

In this paper, the fault-tolerant control technology of the hexarotor UAV in the case of actuator failure is studied, and the fault-tolerant control method is verified by MATLAB simulation and actual flight experiments. This paper mainly completed the following work:

(1) Firstly, this paper studied and established the dynamic and kinematic model of the UAV without fault, which laid a foundation for the attitude control experiment of the UAV.

(2) Secondly, the dynamic and kinematic model of the UAV under fault condition was established, which laid a foundation for the fault-tolerant control experiment of the UAV.

(3) Then, the basic control law and fault-tolerant control law were designed separately.

(4) Finally, the effectiveness of the proposed fault-tolerant control algorithm was verified by simulation experiments and actual flight experiments.

As future work, it is planned to improve the accuracy of the established mathematical models. Furthermore, the fault-tolerant control algorithm will be improved to make it more effective when the UAV takes off and lands.

Data Availability

The data used to support the findings of this study are available from the corresponding author upon request.

Conflicts of Interest

The authors declare that they have no conflicts of interest.

Acknowledgments

References

[1] Q. F. Lin, C. Li, and H. J. Xi, *Development Guide of Embedded Flight Control System for Multi-Rotor UAV*, Tsinghua University Press, Beijing, China, 2017.

[2] Z. Q. Chen, C. L. Wang, and L. Yi, "Design of control system of quadrotor aircraft based on integral sliding mode," *Journal of System Simulation*, vol. 27, pp. 2181–2186, 2015.

[3] Z. Ma, "*Application of active disturbance control technology in quadrotor*," M.S. thesis, North China Electric Power University, Beijing, China, 2018.

[4] X. Y. Cao, C. H. Hu, and J. F. Qiao, "Research on active fault tolerant control of missile actuator based on fault compensation theory," *Electronics Optics & Control*, vol. 20, pp. 30–34, 2013.

[5] X. L. Wang and M. L. Ni, "Fault diagnosis of nonlinear system based on adaptive observer," *Aerospace Control and Application*, vol. 34, pp. 33–37, 2008.

[6] N. P. Nguyen and S. K. Hong, "Fault-tolerant control of quadcopter UAVs using robust adaptive sliding mode approach," *Energies*, vol. 12, no. 1, p. 95, 2018.

[7] M. Wu, "*Research on fault safety system of six-rotor UAV*," M.S. thesis, Nanjing University of Information Science & Technology, Nanjing, China, 2015.

[8] A. Rodic and G. Mester, "Modeling and simulation of quadrotor dynamics and spatial navigation," in *Proceedings of the 2011 IEEE 9th International Symposium on Intelligent Systems and Informatics*, pp. 23–28, Subotica, Serbia, September 2011.

[9] Y. Li, Z. Q. Chen, and Z. X. Liu, "Application of active disturbance rejection technique in attitude control of four-rotor flight," *Journal of Harbin Institute of Technology*, vol. 46, pp. 115–118, 2014.

[10] C. S. Yang, Z. Yang, D. Z. Xu, and L. Ge, "Trajectory tracking control of new six-rotor aircraft," *Systems Engineering and Electronics*, vol. 34, pp. 2098–2150, 2012.

[11] J. Yi, X. Zhang, Z. Ning, and Q. Huang, "Intelligent robot obstacle avoidance system based on fuzzy control," in *Proceedings of the 2009 First International Conference on Information Science and Engineering*, pp. 3812–3815, Nanjing, China, Decemeber 2009.

[12] C. Ha, Z. Zuo, F. B. Choi, and D. Lee, "Passivity-based adaptive backstepping control of quadrotor-type UAVs," *Robotics and Autonomous Systems*, vol. 62, no. 9, pp. 1305–1315, 2014.

[13] X. Xing, X. Chen, L. Huang, and D. Fan, "Study on active fault tolerant flight control systems for quadrotor UAV with actuator failures," *Xibei Gongye Daxue Xuebao/Journal of Northwestern Polytechnical University*, vol. 36, no. 4, pp. 748–753, 2018.

[14] D. Yuan, X. J. Ma, and Q. H. Zeng, "Research on frequency-band characteristics and parameters configuration of linear active disturbance rejection control for second-order system," *Control Theory and Application*, vol. 30, pp. 1630–1640, 2013.

[15] S. B. Li, "*Research on control technology of micro multi-rotor*," M.S. thesis, Nanjing University of Aeronautics and Astronautics, Nanjing, China, 2013.